ISSN 1674-1056
http://cpb.iphy.ac.cn
http://iopscience.iop.org/cpb
中国物理 B
Chinese Physics
中国物理 Chinese Physics B

Effect of laser intensity on quantum trajectories in the macroscopic high-order harmonic generation

Yun Pan(潘云), Fuming Guo(郭福明), Yujun Yang(杨玉军), Dajun Ding(丁大军)
Citation: Chin. Phys. B . 2019, 28(11): 113201 . **doi:** 10.1088/1674-1056/ab47f8
Journal homepage: http://cpb.iphy.ac.cn; http://iopscience.iop.org/cpb

What follows is a list of articles you may be interested in

Helicity of harmonic generation and attosecond polarization with bichromatic circularly polarized laser fields

Jun Zhang(张军), Tong Qi(齐桐), Xue-Fei Pan(潘雪飞), Jing Guo(郭静), Kai-Guang Zhu(朱凯光), Xue-Shen Liu(刘学深)
Chin. Phys. B . 2019, 28(10): 103204 . **doi:** 10.1088/1674-1056/ab4176

Selection of right-circular-polarized harmonics from *p* orbital of neon atom by two-color bicircular laser fields

Chang-Long Xia(夏昌龙), Yue-Yue Lan(兰悦跃), Qian-Qian Li(李倩倩), Xiang-Yang Miao(苗向阳)
Chin. Phys. B . 2019, 28(10): 103203 . **doi:** 10.1088/1674-1056/ab4278

Interpulse interference of electron emission from an atom irradiated by sinusoidally phase-modulated pulse

Hai-Ying Yuan(袁海颖), Fu-Ming Guo(郭福明), Di-Yu Zhang(张頔玉), Jun Wang(王俊), Ji-Gen Chen(陈基根), Yu-Jun Yang(杨玉军)
Chin. Phys. B . 2018, 27(10): 103201 . **doi:** 10.1088/1674-1056/27/10/103201

Simultaneous study of the lower order harmonic and photoelectron emission from an atom in intense laser pulse

Yan Yan(闫妍), Fu-Ming Guo(郭福明), Jun Wang(王俊), Ji-Gen Chen(陈基根), Yu-Jun Yang(杨玉军)
Chin. Phys. B . 2018, 27(8): 083202 . **doi:** 10.1088/1674-1056/27/8/083202

High-order harmonic generation in a two-color strong laser field with Bohmian trajectory theory

Yi-Yi Huang(黄祎祎), Xuan-Yang Lai(赖炫扬), Xiao-Jun Liu(柳晓军)
Chin. Phys. B . 2018, 27(7): 073204 . **doi:** 10.1088/1674-1056/27/7/073204

SPECIAL TOPIC — Strong-field atomic and molecular physics

Effect of laser intensity on quantum trajectories in the macroscopic high-order harmonic generation*

Yun Pan(潘云)[1,2], Fuming Guo(郭福明)[1,2], Yujun Yang(杨玉军)[1,2,†], and Dajun Ding(丁大军)[1,2]

[1] Institute of Atomic and Molecular Physics, Jilin University, Changchun 130012, China

[2] Jilin Provincial Key Laboratory of Applied Atomic and Molecular Spectroscopy (Jilin University), Changchun 130012, China

(Received 20 July 2019; revised manuscript received 5 September 2019; published online 1 November 2019)

We macroscopically investigate the effect of the laser intensity and gas density on quantum trajectories in the high-order harmonic generation of Ne atoms irradiated by few-cycle, 800-nm laser pulses. The time–frequency profile of the harmonics shows that the long quantum trajectory is dominant at both lower and higher gas densities for a low laser intensity. At high laser intensities, the long quantum trajectory plays an important role for lower gas densities, while the short quantum trajectory is dominant at higher gas densities. An analysis of the phase mismatch for high-order harmonic generation shows that the primary emission of the quantum trajectories is determined by dynamic changes in the laser electric field during the propagation process.

Keywords: high-order harmonic generation, quantum trajectory

PACS: 32.80.Rm, 42.50.Hz **DOI:** 10.1088/1674-1056/ab47f8

1. Introduction

High-order harmonics generated by the interaction of intense lasers with atoms or molecules have been extensively studied and provide an effective scheme for achieving attosecond pulses.[1–8] High-order harmonic generation (HHG) is a highly nonlinear process governed by the dynamic response of atoms in a gaseous medium under the action of a driving laser pulse. The HHG measured in an experiment is the collective response of all atoms in the macroscopic medium. The intensity of the high-order harmonics is sensitive to the driving laser parameters and the properties of the gaseous medium.[9–14] At present, the application of HHG is limited by a low emission intensity. To increase the emission intensity, one effective method is to generate favorable phase-matching conditions during HHG.

By adjusting the position of the gas target relative to the laser focus as well as the gas density, laser intensity, and other macroscopic parameters, good phase matching can be achieved. The effect of these macroscopic parameters on HHG can be reflected by the long and short quantum trajectories.[15] Previous studies have generally concluded that the long quantum trajectory is dominant when the gas target is located before the laser focus, while the short quantum trajectory is dominant when the gas target is located after the laser focus. For example, in 2011, Vozzi *et al.* applied a 1500-nm, 20-fs laser pulse to Xe atoms and observed that when the gas target was located before the laser focus, the long quantum trajectory dominated; moreover, when the gas target was located after the laser focus, the short quantum trajectory dominated.[16] In 2014, Hutchison *et al.* applied an 800-nm laser and an orthogonally polarized second-order harmonic field to Ar atoms.[17] The authors found that when the gas target was in front of the laser focus, the short quantum trajectory on the axis played a greater role, while the long quantum trajectory off the axis was dominant. The harmonic emissions of the long and short quantum trajectories can be separated, and in some cases, intermediate rings generated by the interference of the quantum trajectories can be observed. In the same year, Ye *et al.* applied an 800-nm, 4.2-fs pulse to Ne atoms and found that when the gas chamber was located before the laser focus, the effect of the long quantum trajectory was prominent; in contrast, when the gas chamber was located after the laser focus, the effect of the short quantum trajectory was prominent.[15]

However, in our recent work, we found that when the center of the gas target is located at the laser focus, an ultra-short laser pulse can undergo significant reshaping as the gas density increases at moderate laser intensities.[18] The long quantum trajectory is effective for phase matching at low gas density, while the short quantum trajectory is effective for phase matching at high gas density. Thus, the effects of the long and short quantum trajectories are not simply determined by the position of the gas target relative to the laser focus. The effect

*Project supported by the National Key Research and Development Program of China (Grant No. 2017YFA0403300), the National Natural Science Foundation of China (Grant Nos. 11627807, 11774175, 11534004, 11774129, and 11604119), the Fundamental Research Funds for the Central Universities of China (Grant No. 30916011207), the Jilin Provincial Research Foundation for Basic Research, China (Grant No. 20170101153JC), and the Science and Technology Project of the Jilin Provincial Education Department, China (Grant No. JJKH20190183KJ).

†Corresponding author. E-mail: yangyj@jlu.edu.cn

© 2019 Chinese Physical Society and IOP Publishing Ltd

of the laser intensity on the quantum trajectory is also an important factor to consider for HHG, in addition to the position of the gas target center relative to the laser focus. The main purpose of this work is to study the effect of the laser intensity on quantum trajectories in the macroscopic HHG process at different gas densities.

In this study, the single-atom response is obtained from the quantitative re-scattering (QRS) model,[19] and the macroscopic effect is considered by applying Maxwell's wave equations.[20] In the simulations, a few-cycle 800-nm laser interacts with Ne atoms. The results indicate that the laser intensity and gas density affect the harmonic emission of the long and short quantum trajectories. For a lower laser intensity, phase matching of the long quantum trajectory dominates at lower and higher gas densities. In contrast, for a higher laser intensity, phase matching of the long quantum trajectory dominates at lower gas densities, while phase matching of the short quantum trajectory can be achieved at higher densities.

2. Theoretical methods

2.1. Single-atom model

In the QRS theory, the induced dipole moment $D(\omega)$ of an atom is expressed as[19,20]

$$D(\omega) = W^{\mathrm{SFA}}(E)\, d(\omega), \tag{1}$$

where $W^{\mathrm{SFA}}(E)$ is the return electron wave packet calculated by the strong field approximation (SFA), E represents the electron energy, $d(\omega)$ is the light recombination transition dipole matrix element, and ω represents the emitted photon energy.

The return electron wave packet is written as

$$W^{\mathrm{SFA}}(E) = \frac{D^{\mathrm{SFA}}(\omega)}{d^{\mathrm{PWA}}(\omega)}, \tag{2}$$

where $D^{\mathrm{SFA}}(\omega)$ is the induced dipole moment calculated by the SFA and $d^{\mathrm{PWA}}(\omega)$ is the transition dipole obtained by the plane wave approximation (PWA). Then, the induced dipole moment can be expressed as

$$D(\omega) = \frac{d(\omega)}{d^{\mathrm{PWA}}(\omega)} D^{\mathrm{SFA}}(\omega). \tag{3}$$

2.2. Propagation model

In the ionization medium, we obtain the collective response of the macroscopic gases by numerically solving Maxwell's wave equations for the driving laser field E_1 and the harmonic field E_{h}[21–24]

$$\nabla^2 E_1(r,z,t) - \frac{1}{c^2}\frac{\partial^2 E_1(r,z,t)}{\partial t^2} = \mu_0 \frac{\partial J_{\mathrm{abs}}(r,z,t)}{\partial t} + \frac{\omega_{\mathrm{p}}^2}{c^2} E_1(r,z,t) - 2\frac{\omega_0^2}{c^2}\left(\delta_1 + \eta_2 I(r,z,t)\right) E_1(r,z,t), \tag{4}$$

$$\nabla^2 E_{\mathrm{h}}(r,z,t) - \frac{1}{c^2}\frac{\partial^2 E_{\mathrm{h}}(r,z,t)}{\partial t^2} = \mu_0 \frac{\partial^2 P(r,z,t)}{\partial t^2}, \tag{5}$$

where c is the speed of light, μ_0 is the permeability of free space, ω_0 is the fundamental field frequency, and ω_{p} is the plasma frequency. δ_1 is the refraction coefficient of the neutral atoms, which depends on the temperature and pressure of the gas medium. η_2 is the nonlinear refractive index, which depends on the gas pressure. $I(r,z,t)$ is the laser intensity and $P(r,z,t)$ is a polarization term associated with the laser field $E_1(r,z,t)$, where r is the radial position perpendicular to the propagation direction and z is the position along the propagation direction. $J_{\mathrm{abs}}(r,z,t)$ is the absorption term of the ionization medium, which can be expressed as[25,26]

$$J_{\mathrm{abs}}(r,z,t) = \frac{\gamma(r,z,t)\left(n_0 - n_{\mathrm{e}}(r,z,t)\right) I_{\mathrm{p}} E_1(r,z,t)}{|E_1(r,z,t)|^2}, \tag{6}$$

where $\gamma(r,z,t)$ is the ionization rate, which can be given by the Ammosov–Delone–Krainov (ADK) theory.[27] n_0 is the neutral atom density and $n_{\mathrm{e}}(r,z,t) = n_0\{1 - \exp[-\int_0^t \gamma(r,z,\tau)\mathrm{d}\tau]\}$ is the density of the ionized electrons.[28] I_{p} is the ionization energy of the atom.

The plasma frequency is

$$\omega_{\mathrm{p}}(r,z,t) = \left[e^2 n_{\mathrm{e}}(r,z,t)/(\varepsilon_0 m_{\mathrm{e}})\right]^{1/2}, \tag{7}$$

where e is the charge of an electron, m_{e} is the mass of an electron, and ε_0 is the vacuum permittivity. We use the Crank–Nicolson method to solve Eqs. (4) and (5).

2.3. Phase mismatch of harmonics

The phase mismatch is usually used for analyzing macroscopic harmonics, which can be expressed as[29,30]

$$\Delta k = \Delta k_{\mathrm{g}} + \Delta k_{\mathrm{p}} + \Delta k_{\mathrm{n}} + \Delta k_{\mathrm{d}}, \tag{8}$$

where

$$\Delta k_{\mathrm{g}} = \frac{1}{1 + (z/z_{\mathrm{R}})^2} \cdot \frac{q}{z_{\mathrm{R}}} + 2qk_0 r^2 \frac{z^2 - z_{\mathrm{R}}^2}{\left(2z^2 + 2z_{\mathrm{R}}^2\right)^2}$$

is the phase mismatch caused by the geometric phase of the Gaussian beam, q is the harmonic order, k_0 is the wave vector of the fundamental frequency field, and $z_{\mathrm{R}} = \pi w_0^2/\lambda_0$ is the Rayleigh length, with λ_0 being the laser wavelength. $\Delta k_{\mathrm{p}} = \eta p N_{\mathrm{atm}} r_{\mathrm{e}} \lambda_0 (1//q - q)$ is the phase mismatch caused by the plasma dispersion, η is the ionization probability, p is the gas pressure, N_{atm} is the gas atomic number density under standard conditions, and r_{e} is the classical electron radius. $\Delta k_{\mathrm{n}} = \frac{2\pi q}{\lambda_0} p\delta_{\mathrm{n}}(1-\eta)$ is the phase mismatch caused by the dispersion of the medium and $\delta_{\mathrm{n}} = n_{\mathrm{laser}} - n_{\mathrm{harmonic}}$ is the

difference in the refractive index of the gas per unit atmospheric pressure between the fundamental wavelength and the harmonic wavelength. $\Delta k_{\rm d} = \alpha_{\rm i}\partial I/\partial z$ is the phase mismatch caused by the intensity-dependent single-atom dipole phase, where $\alpha_{\rm i}$ is a phase coefficient; for the long quantum trajectory, $\alpha_{\rm i} = 24 \times 10^{-14}$ cm^2/W, and for the short quantum trajectory, $\alpha_{\rm i} = 1 \times 10^{-14}$ cm^2/W.

3. Results and discussion

In the calculations, the driving laser field parameters are as follows. The wavelength is 800 nm, the pulse duration is 4 fs, and the laser beam waist is 25 μm. The length of the gas target is 1 mm and the gas target center is located 1 mm before the laser focus. An Ne atom is used as the target atom. We show the changes in macroscopic HHG spectra for varying gas densities and four laser intensities in Fig. 1. First, at a low laser intensity of 2×10^{14} W/cm^2, as the gas density increases, the efficiencies of the harmonics and the cut-off energies of the harmonic spectra remain almost constant, as shown in Fig. 1(a). As shown in Figs. 1(a)–1(d), the efficiencies of the harmonics increase significantly as the laser intensity increases. At higher laser intensities, as the gas density increases, the efficiencies of the harmonics first increase and then decrease, while the cut-off energies gradually decrease. Clearly, there is an optimal balance between the efficiencies of the harmonics in the plateau and the cut-off energies at a certain gas density; the efficiency of the harmonic is higher and the cut-off energy is larger at this gas density, which is denoted as the optimum gas density. The green dotted lines in Fig. 1 present the HHG spectra at the optimum gas density for each laser intensity.

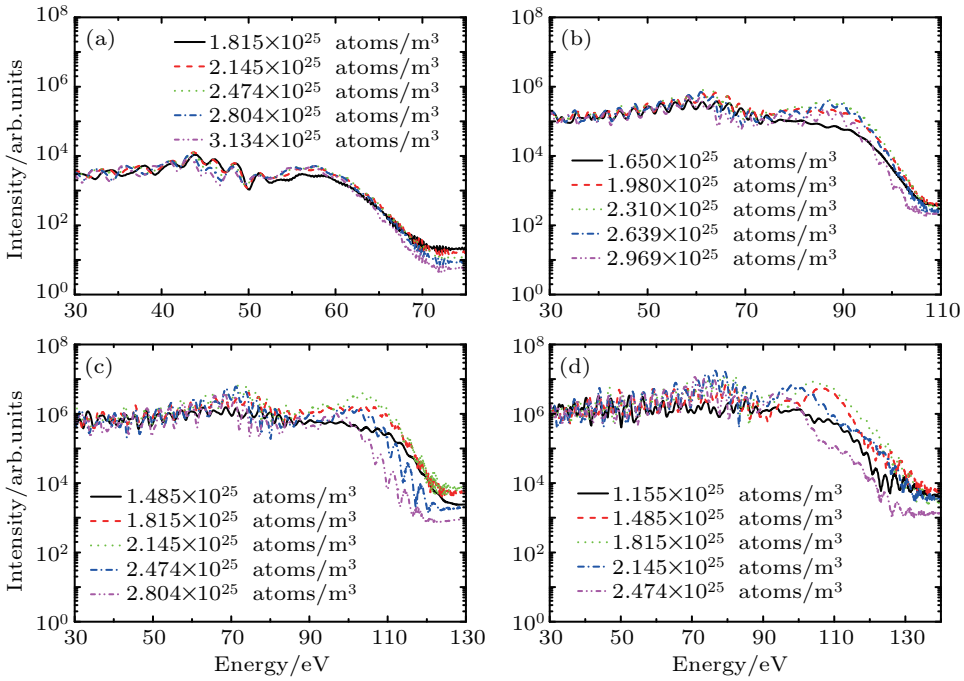


Fig. 1. Macroscopic HHG spectra for different gas densities at four laser intensities: (a) 2×10^{14} W/cm^2, (b) 4×10^{14} W/cm^2, (c) 6×10^{14} W/cm^2, and (d) 8×10^{14} W/cm^2. The green dotted lines present HHG spectra measured at the optimum gas density for each laser intensity.

To understand the variation in the HHG spectra with laser intensity and gas density shown in Fig. 1, we carefully studied the time-frequency profiles of the near-field harmonics on the end surface of the gas target at lower and higher gas densities for different laser intensities, as shown in Fig. 2. For a laser intensity of 2×10^{14} W/cm^2, at both a lower gas density of 1.815×10^{25} atoms/m^3 and a higher gas density of 3.134×10^{25} atoms/m^3, between 0 and 1.0 optical cycle (o.c.), there is only one primary emission burst per half optical period with a negative chirp, which is generated by the long quantum trajectory, and the corresponding electron ionization occurs between −0.5 and 0.5 o.c. Meanwhile, the positive chirp emission is very weak, indicating that the long quantum trajectory contributes to the emission of the harmonics, as shown in Figs. 2(a) and 2(b). For a laser intensity of 4×10^{14} W/cm^2 at both a lower gas density of 1.650×10^{25} atoms/m^3 and a higher gas density of 2.969×10^{25} atoms/m^3 and for a laser intensity of 6×10^{14} W/cm^2 at a lower gas density of 1.485×10^{25} atoms/m^3, between 0 and 1.0 o.c., there is one emission burst with two branches per half optical period. The positive chirp emission is generated by the short quantum trajectory and the negative chirp emission is generated by the long quantum trajectory, as shown in Figs. 2(c)–2(e). The corresponding electron ionization occurs between −0.5 and 0.5 o.c. However, the emission intensities of the positive and negative chirps between 0 and 0.5 o.c. are similar, indicat-

ing that the short and long quantum trajectories both contribute to the harmonic emission. The negative chirp emission between 0.5 and 1.0 o.c. is significantly greater than the positive chirp emission, implying that the long quantum trajectory is more favorable to the harmonic emission. For a laser intensity of 6×10^{14} W/cm^2 at a higher gas density of 2.969×10^{25} atoms/m^3, between 0 and 1.0 o.c., we observe one emission burst with two branches per half optical period. However, the negative chirp emission is weak and the positive chirp emission dominates, as shown in Fig. 2(f), indicating that the stronger harmonic emission comes from the short quantum trajectory. As the laser intensity is further increased to 8×10^{14} W/cm^2, for both a lower gas density of 1.155×10^{25} atoms/m^3 and a higher gas density of 2.474×10^{25} atoms/m^3, the negative chirp emission is clearly caused by the long quantum trajectory and the positive chirp caused by the short quantum trajectory is dominant, as shown in Figs. 2(g) and 2(h), respectively. As the laser intensity increases, the effects of the long and short quantum trajectories differ significantly at lower and higher gas densities.

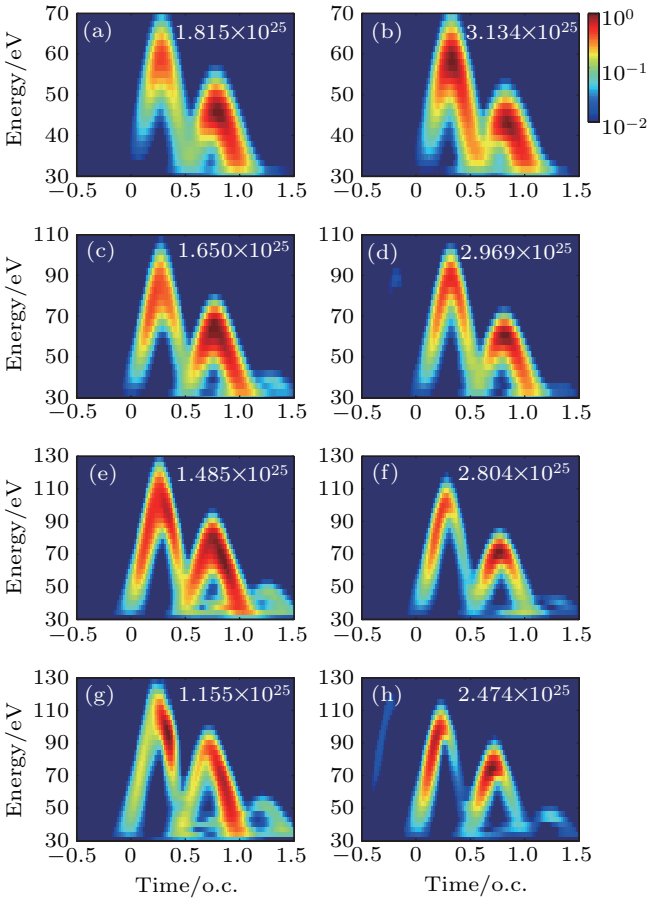


Fig. 2. Time–frequency profiles of HHG on the end surface of the gas target at lower and higher gas densities for different laser intensities: (a) and (b) 2×10^{14} W/cm^2, (c) and (d) 4×10^{14} W/cm^2, (e) and (f) 6×10^{14} W/cm^2, (g) and (h) 8×10^{14} W/cm^2.

Figure 2 only shows information regarding the near-field harmonic emissions on the end surface of the gas target. To understand the mechanism governing the dominant quantum trajectory for a given laser intensity and gas density, we must assess how the harmonic emissions accumulate during propagation in the gas target. In Fig. 3, we show the time–frequency profiles of HHG for selected planes perpendicular to the direction of propagation at different gas densities for two laser intensities. The results for $z=-0.5$ mm are shown in Fig. 2. Figures 3(a)–3(d) correspond to a laser intensity of 2×10^{14} W/cm^2 and a gas density of 1.815×10^{25} atoms/m^3, figures 3(e)–3(h) correspond to a laser intensity of 8×10^{14} W/cm^2 and a gas density of 1.155×10^{25} atoms/m^3, and figures 3(i)–3(l) correspond to a laser intensity of 8×10^{14} W/cm^2 and a gas density of 2.474×10^{25} atoms/m^3. Figures 3(a), 3(e), and 3(i) show the harmonic emissions at the initial surface of the gas target for three conditions, which all reflect the emission characteristics of a single atom. For a laser intensity of 2×10^{14} W/cm^2 and a gas density of 1.815×10^{25} atoms/m^3, two primary emission bursts are observed between 0 and 1.0 o.c., and the long quantum trajectory is clearly dominant. As the harmonic field continues to accumulate, the cut-off energy of the harmonics increases significantly. Moreover, the normalization factor indicates that the intensities of the harmonics also increase significantly. However, the relative strengths of the long and short quantum trajectories remain nearly constant, as shown in Figs. 3(a)–3(d). In contrast to the case of low laser intensity, for a high laser intensity of 8×10^{14} W/cm^2, two primary emission bursts occur between 0 and 1.0 o.c. regardless of the gas density, indicating that the long and short quantum trajectories exist simultaneously. At a low gas density of 1.155×10^{25} atoms/m^3, the harmonic intensities increase with the accumulation of the harmonic fields. The emissions of the long and short quantum trajectories from 0 to 0.5 o.c. are obviously enhanced, while the emission of the short quantum trajectory is weakened from 0.5 to 1.0 o.c., as shown in Fig. 3(f). Figures 3(f)–3(h) show that the short quantum trajectory is weakened near 0 and 0.5 o.c., while the long quantum trajectory dominates near 0.3 and 1.0 o.c. In Figs. 3(h)–3(l), the harmonic emission structure is very stable. At a high gas density of 2.474×10^{25} atoms/m^3, the short quantum trajectory between 0 and 0.5 o.c. becomes dominant as the harmonic field gradually accumulates, and the long and short quantum trajectories are equivalent between 0.5 and 1.0 o.c., as shown in Fig. 3(j). The intensities of the long and short quantum trajectories between 0.5 and 1.0 o.c. are almost the same, as shown in Fig. 3(j). In Figs. 3(j)–3(l), the short quantum trajectory is still dominant between 0 and 0.5 o.c.; meanwhile, the long quantum trajectory gradually weakens between 0.5 and 1.0 o.c., and the short quantum trajectory gradually becomes dominant. In Fig. 3(l), the harmonic emission behavior is very stable. Thus, the cut-off energies of the harmonics are significantly reduced during the propagation process.

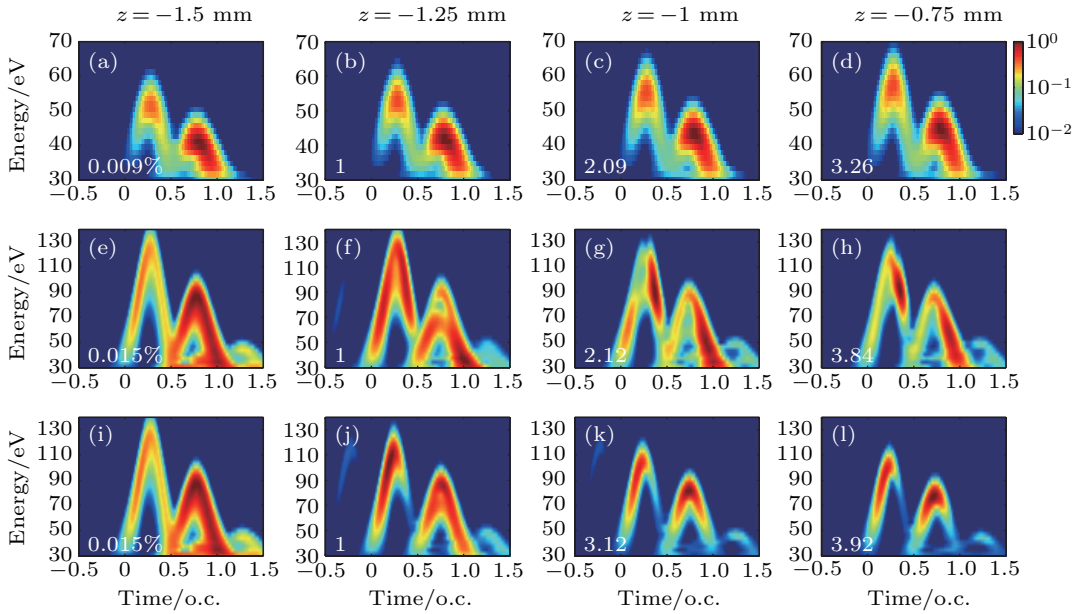


Fig. 3. Evolution of the time–frequency profiles of harmonic emissions along the direction of laser propagation. The laser intensities and gas densities are as follows: (a)–(d) 2×10^{14} W/cm^2, 1.815×10^{25} atoms/m^3, (e)–(h) 8×10^{14} W/cm^2, 1.155×10^{25} atoms/m^3, (i)–(l) 8×10^{14} W/cm^2, 2.474×10^{25} atoms/m^3. The harmonic efficiency of each position is independently normalized, and the normalization coefficient is given in the lower left corner.

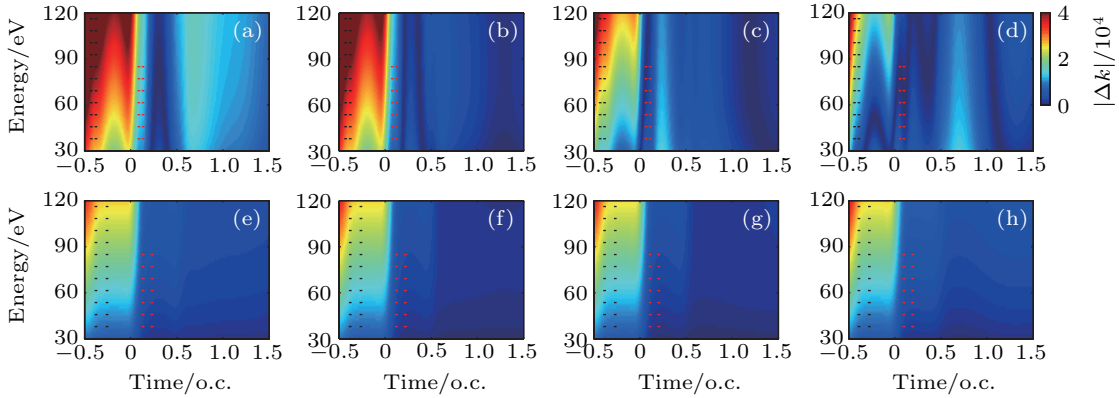


Fig. 4. Evolution of the total phase mismatch $|\Delta k|$ of the off-axis HHG along the propagation direction ($z=-1.25$ mm, -1 mm, -0.75 mm, -0.5 mm): (a)–(d) long quantum trajectory, (e)–(h) short quantum trajectory. The laser intensity is 8×10^{14} W/cm^2, and the gas density is 1.155×10^{25} atoms/m^3.

To further elucidate the results presented in Fig. 1, we first performed a detailed analysis for a laser intensity of 8×10^{14} W/cm^2 and a gas density of 1.155×10^{25} atoms/m^3. Figure 4 shows the evolution of the total phase mismatch $|\Delta k|$ of the off-axis ($r=w/3$) HHG along the propagation direction. The blue (red) region corresponds to good (poor) phase matching. The time interval of the black dotted line (red dotted line) frames in Figs. 4(a)–4(d) corresponds to the ionization time of the emission of the long quantum trajectory between 0 and 0.5 o.c. (0.5 and 1.0 o.c.) in Figs. 3(e)–3(h). The time interval of the black dotted line (red dotted line) frames in Figs. 4(e)–4(h) corresponds to the ionization time of the emission of the short quantum trajectory between 0 and 0.5 o.c. (0.5 and 1.0 o.c.) in Figs. 3(e)–3(h). By comparing Fig. 4(a) with Fig. 4(e), it can be seen that at $z=-1.25$ mm, within the black dotted line frame, the phase mismatch of the harmonics of the long quantum trajectory is greater than that of the short quantum trajectory, resulting in a greater contribution to the harmonics from the short quantum trajectory. The phase mismatches of the harmonics for the electrons emitted by the long and short quantum trajectories in the red dotted line frame are comparable, leading to similar contributions to the harmonics from the long and short quantum trajectories. This finding is consistent with the time–frequency profile of HHG presented in Fig. 3(f). As the harmonic field propagates forward, we find that the phase mismatch of the harmonics of the long quantum trajectory gradually decreases, as shown in Figs. 4(a)–4(d); however, the phase mismatch remains nearly constant for the short quantum trajectory, as shown in Figs. 4(e)–4(h). Thus, the long quantum trajectory becomes dominant during the process of propagation. For a laser intensity of 2×10^{14} W/cm^2 and a gas density of 1.815×10^{25} atoms/m^3 and for a laser intensity of 8×10^{14} W/cm^2 and a gas density of 2.474×10^{25} atoms/m^3, the total phase mismatch $|\Delta k|$ of the off-axis HHG along the

propagation direction is shown in Figs. 5 and 6, corresponding to the evolution of the time–frequency profiles of the HHG in Figs. 3(a)–3(d) and 3(i)–3(l), respectively. For a lower laser intensity of 2×10^{14} W/cm^2, the phase mismatch of the harmonics of the long quantum trajectory gradually decreases, and thus, the long quantum trajectory is dominant for the HHG. For a laser intensity of 8×10^{14} W/cm^2 and a gas density of 2.474×10^{25} atoms/m^3, the phase mismatch of the harmonics of the short quantum trajectory remains nearly constant and is always smaller than that of the long quantum trajectory, which results in the dominance of the short quantum trajectory during propagation.

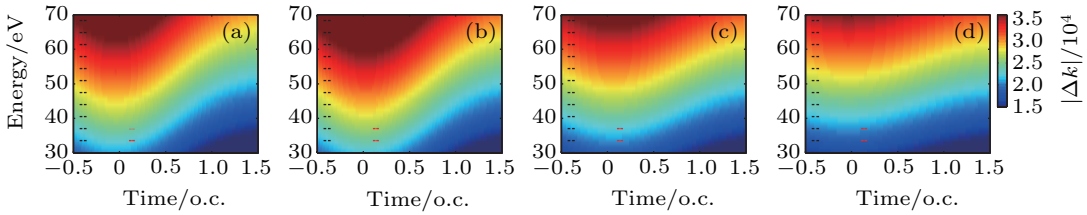


Fig. 5. Evolution of the total phase mismatch $|\Delta k|$ of the off-axis HHG along the propagation direction ($z=-1.25$ mm, -1 mm, -0.75 mm, -0.5 mm). The laser intensity is 2×10^{14} W/cm^2, and the gas density is 1.815×10^{25} atoms/m^3.

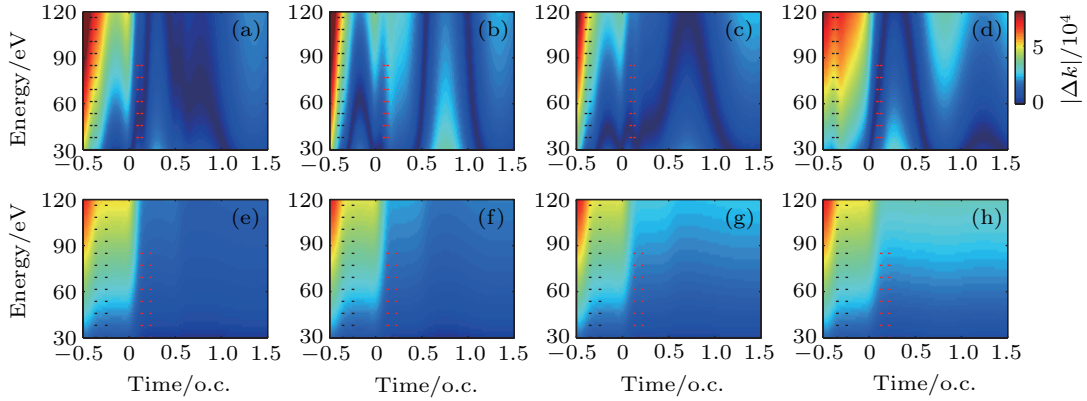


Fig. 6. The results presented here correspond to those presented in Fig. 4 for a gas density of 2.474×10^{25} atoms/m^3.

Next, we will further explore the contribution of the individual components of the HHG phase mismatch to the total phase mismatch, namely, $\Delta k_{\rm g}$, $\Delta k_{\rm p}$, $\Delta k_{\rm n}$, and $\Delta k_{\rm d}$, to determine which factor plays a key role in the change of the total phase mismatch, which in turn affects the harmonics. The off-axis electric field of the 800-nm laser beam and the spatial distribution of the ionized electron density are shown in Fig. 7 for three different conditions. The variation in the harmonic cut-off energy shown in Fig. 3 can be well understood from the evolution of the electric field. For a lower laser intensity of 2×10^{14} W/cm^2, as the laser field propagates forward along the z direction, the laser electric field and the ionized electron density gradually increase, as shown in Figs. 7(a) and 7(d). This behavior also explains the increase in the harmonic cut-off energy during the evolution of the HHG time–frequency profiles shown in Figs. 3(a)–3(d). However, the ionized electron density is approximately five orders of magnitude smaller than the neutral atom density, which leads to a negligible contribution of $\Delta k_{\rm p}$, and the other three terms are all positive, where $\Delta k_{\rm g}$ is the influence of the Gouy phase shift of the Gaussian beam, which is constant for a given system. Because the ionized electron density is very low, the change in the neutral atom density can be ignored. As the harmonic field propagates forward, the contributions of $\Delta k_{\rm g}$ and $\Delta k_{\rm n}$ remain unchanged, and $\Delta k_{\rm d}$ depends on the change in laser intensity. From the evolution of the laser electric field shown in Fig. 7(a), it can be seen that the change in the laser electric field with the change in propagation distance decreases; thus, the contribution of $\Delta k_{\rm d}$ and the total phase mismatch each gradually decrease. For a higher laser intensity of 8×10^{14} W/cm^2 and a lower gas density of 1.155×10^{25} atoms/m^3, the ionized electron density shows little change as the laser field propagates forward, as shown in Fig. 7(e), which causes the contributions of $\Delta k_{\rm p}$ and $\Delta k_{\rm n}$ to remain nearly constant. However, from the evolution of the field shown in Fig. 7(b), it can be seen that the laser electric field first increases slightly and then decreases slightly, which leads to a gradual change in $\Delta k_{\rm d}$ from positive to negative. As the harmonic field propagates, the contributions of $\Delta k_{\rm g}$ and $\Delta k_{\rm n}$ are positive, the contribution of $\Delta k_{\rm p}$ is negative, and $\Delta k_{\rm p}$ and $\Delta k_{\rm d}$ can compensate for the mismatch caused by $\Delta k_{\rm g}$ and $\Delta k_{\rm n}$. Moreover, because the orbital coefficient $\alpha_{\rm i}$ of the long quantum trajectory is more than 20 times greater than that of the short quantum trajectory, the contribution of the $\Delta k_{\rm d}$ term of the short quantum trajectory

is very small, which leads to a gradual decrease in the total phase mismatch for the long quantum trajectory. However, the total phase mismatch for the short quantum trajectory remains nearly constant as the harmonic field propagates, which is consistent with the description presented in Fig. 4. At a higher gas density of 2.474×10^{25} atoms/m^3, as the laser field propagates forward from $z = -1.5$ mm to $z = -1$ mm, the laser electric field and ionized electron density gradually decrease, and from $z = -1$ mm to $z = -0.5$ mm, these parameters tend to be stable, as shown in Figs. 7(c) and 7(f). The decrease in the laser electric field directly explains the decrease in the harmonic cut-off energy in the evolution of the HHG time–frequency profiles shown in Figs. 3(i)–3(l). From $z = -1.5$ mm to z$= -1$ mm, the density of the ionized electrons is very large. At this point, as z increases, $\Delta k_{\rm g}$ and $\Delta k_{\rm n}$ compensate for the mismatch caused by $\Delta k_{\rm p}$ and $\Delta k_{\rm d}$. Thus, the phase mismatch for the short quantum trajectory in this process is small. From $z = -1$ mm to $z = -0.5$ mm, the laser electric field tends to be stable, and the contribution of $\Delta k_{\rm d}$ can be ignored. Therefore, the phase matching remains unchanged, consistent with the description given in Fig. 6.

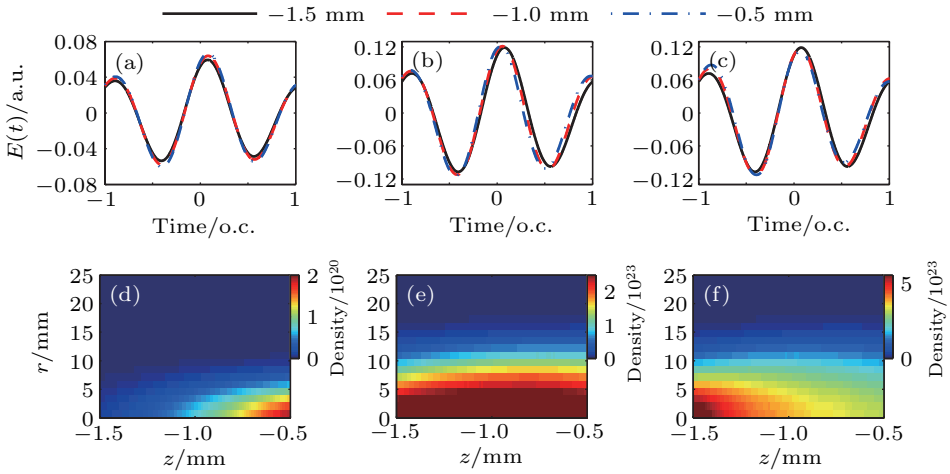


Fig. 7. Off-axis electric field of the 800-nm laser beam and the spatial distribution of the ionized electron density under three different conditions. (a) and (d) Laser intensity of 2×10^{14} W/cm^2 and a gas density of 1.815×10^{25} atoms/m^3. (b) and (e) Laser intensity of 8×10^{14} W/cm^2 and a gas density of 1.155×10^{25} atoms/m^3. (c) and (f) Laser intensity of 8×10^{14} W/cm^2 and a gas density of 2.474×10^{25} atoms/m^3.

4. Conclusion and perspectives

We macroscopically studied the effect of the laser intensity on the quantum trajectory in macroscopic harmonic spectra. By analyzing the time–frequency evolution of the harmonic emissions during propagation, we found that the long quantum trajectory at low laser intensities is dominant at both lower and higher gas densities; in contrast, for high laser intensities, the long quantum trajectory dominates at lower gas density while the short quantum trajectory dominates at higher gas density. By using the phase-mismatch formulation, we evaluated the effect of the laser intensity and gas density on the conditions for generating short or long quantum trajectories. In order to observe the motions of electrons, it is necessary to generate an isolated attosecond pulse in experiment. Through this theoretical calculation, it is possible to select the long or short quantum emission trajectories for the generation of isolated attosecond pulse by optimizing the gas density.

Acknowledgement

We acknowledge the High-Performance Computing Center of Jilin University for supercomputer time.

References

[1] Spielmann C, Burnett N H, Sartania S, Koppitsch R, Schnurer M, Kan C, Lenzner M, Wobrauschek P and Krausz F 1997 *Science* **278** 661
[2] Takahashi E J, Kanai T, Ishikawa K L, Nabekawa Y and Midorikawa K 2008 *Phys. Rev. Lett.* **101** 253901
[3] Xiong H, Xu H, Fu Y, Yao J, Zeng B, Chu W, Cheng Y, Xu Z, Takahashi E J, Midorikawa K, Liu X and Chen J 2009 *Opt. Lett.* **34** 1747
[4] Chen M C, Arpin P, Popmintchev T, Gerrity M, Zhang B, Seaberg M, Popmintchev D, Murnane M M and Kapteyn H C 2010 *Phys. Rev. Lett.* **105** 173901 (in Chinese)
[5] Sorensen S L, Bjorneholm O, Hjelte I, Kihlgren T, Ohrwall G, Sundin S, Svensson S, Buil S, Descamps D and L'Huillier A 2000 *J. Chem. Phys.* **112** 8038
[6] Krausz F and Ivanov M 2009 *Rev. Mod. Phys.* **81** 163
[7] Zhang H D, Guo J, Shi Y, Du H, Liu H F, Huang X R, Liu X S, and Jing J 2017 *Chin. Phys. Lett.* **34** 014206
[8] Zhang B, Zhao J, and Zhao Z X 2018 *Chin. Phys. Lett.* **35** 043201
[9] Popmintchev T, Chen M C, Popmintchev D, Arpin P, Brown S, Ališauskas S, Andriukaitis G, Balciunas T, Mücke O D, Pugzlys A, Baltuška A, Shim B, Schrauth S E, Gaeta A, Hernández-García C, Plaja L, Becker A, JaronBecker A, Murnane M M and Kapteyn H C 2012 *Science* **336** 1287
[10] Jin C and Lin C D 2012 *Phys. Rev. A* **85** 033423
[11] Brizuela F, Heyl C M, Rudawski P, Kroon D, Rading L, Dahlström J M, Mauritsson J, Johnsson P, Arnold C L and L'Huillier A 2013 *Sci. Rep.* **3** 01410
[12] He L X, Lan P F, Zhang Q B, Zhai C Y, Wang F, Shi W J and Lu P X 2015 *Phys. Rev. A* **92** 043403
[13] Li Q G, Lan P F, Hong W Y, Zhang Q B, and Lu P X 2009 *Acta Phys. Sin.* **58** 8 (in Chinese)
[14] Lu Y Y, Zeng Z N, Zheng Y H, Zou P, Liu C D, Gong C, Li R X and Xu Z Z 2011 *Acta Phys. Sin.* **60** 103202 (in Chinese)

[15] Ye P, He X, Teng H, Zhan M, Zhong S, Zhang W, Wang L and Wei Z 2014 *Phys. Rev. Lett.* **113** 073601
[16] Vozzi C, Negro M, Calegari F, Stagira S, Kovács K and Tosa V 2011 *New J. Phys.* **13** 073003
[17] Hutchison C, Houver S, Lin N, Hoffmann D J, McGrath F, Siegel T, Austin D R, Zaïr A, Salières P and Marangos J P 2014 *J. Mod. Opt.* **61** 608
[18] Pan Y, Guo F M, Jin C, Yang Y J and Ding D J 2019 *Phys. Rev. A* **99** 033411
[19] Le A T, Morishita T and Lin C D 2008 *Phys. Rev. A* **78** 023814
[20] Jin C, and Lin C D 2016 *Chin. Phys. B* **25** 094213
[21] Jin C, Le A T and Lin C D 2011 *Phys. Rev. A* **83** 023411
[22] Geissler M, Tempea G, Scrinzi A, Schnürer M, Krausz F and Brabec T 1999 *Phys. Rev. Lett.* **83** 2930
[23] Priori E, Cerullo G, Nisoli M, Stagira S, Silvestri S D, Villoresi P, Poletto L, Ceccherini P, Altucci C, Bruzzese R and Lisio C D 2000 *Phys. Rev. A* **61** 063801
[24] Takahashi E, Tosa V, Nabekawa Y and Midorikawa K 2003 *Phys. Rev. A* **68** 023808
[25] Gaarde M B, Tate J L and Schafer K J 2008 *J. Phys. B* **41** 132001
[26] Rae S C and Burnett K 1992 *Phys. Rev. A* **46** 1084
[27] Popov V S 2004 *Phys. Usp.* **47** 855
[28] Tong X M and Lin C D 2005 *J. Phys. B* **38** 2593
[29] Averchi A, Faccio D, Berlasso R, Kolesik M, Moloney J V, Couairon A and Trapani P D 2008 *Phys. Rev. A* **77** 021802
[30] Pfeifer T, Spielmann C and Gerber G 2006 *Rep. Prog. Phys.* **69** 443